Supplementary materials

Unlocking lattice oxygen mobility via acid etching in $Co_3O_4/CeZrO_2$ for efficient passive NO_x adsorption

*Yan Huang [a], Yan Li [b], Chengsong Huang [a], Jianli Wang [b], Yaoqiang Chen [b], Haidi Xu [a,] **

[a] Institute of New Energy and Low-Carbon Technology, Sichuan University, Chengdu 610064 Sichuan, P.R. China

[b] Sichuan Provincial Environmental Protection Environmental Catalytic Materials Engineering Technology Center, College of Chemistry, Sichuan University, Chengdu 610064 Sichuan, P.R. China

* Corresponding Authors: Tel. /Fax: +86-28-85418451

* E-mail: xuhaidi@scu.edu.cn

Section S1: Catalytic performance measurement

The concentration of N_xO_y was monitored using Fourier Transform Infrared Spectroscopy (FTIR, Antaris IGS, Nicolet, USA). The experimental procedure was as follows: (1) The sample was loaded into the reaction tube and treated under N_2 flow at 500 °C for 1 h. (2) The sample was subsequently cooled to 120 °C for NO + O_2 / NO adsorption, which was conducted for 20 min. (3) After adsorption, the gas flow was switched to N_2 to purge the system until the N_xO_y concentration fell below 10 ppm. (4) Temperature-programmed desorption (TPD) was performed by heating the sample from 120 °C to 500 °C at a rate of 10 °C/min. The NO_x adsorption capacity (NAC) and desorption capacity (NSC) were calculated according to the following formulas

$$NAC(\mu mol/g) = \frac{(\int_0^{t1} NO_{x,in} - NO_{x,out}dt)V}{22.4 \times m}$$

$$NSC(\mu mol/g) = \frac{(\int_0^{t2} NO_{x,out}dt)V}{22.4 \times m}$$

$NO_{x,in}$ (ppm) — initial concentration of NO_x in the gas mixture.

$NO_{x,out}$ (ppm) — outlet concentration of NO_x in the gas mixture.

m(g) — the weight of PNA.

t_1 (min) — the duration of storage process.

t_2(min) — the duration of desorption process.

V(mL/min)—gas flow rate.

Section S2: Catalyst characterization

X-ray diffraction (XRD) measurements were carried out on a Rigaku DX-2500 diffractometer (Rigaku, Japan) using Cu-Kα radiation (λ = 0.15406 nm). Powder diffraction patterns were collected over a 2θ range of 10–80° at a scanning rate of 8°/min, with the X-ray tube operated at 40 kV and 25 mA.

Specific surface areas were calculated using the Bruner-Emmett-Teller (BET) method and pore volumes were calculated using the Barrett-Joyner-Halenda (BJH) method. The sample was pretreated at 300 °C for 3 h, followed by N_2 adsorption–desorption measurements at 77 K.

Visible Raman spectroscopy (Vis-Raman) were obtained on an inVia-Qontor system (Renishaw, UK) with 532 nm excitation wavelength and the laser power of 50 mW. The detection range of 100-2000 cm^{-1}.

Inductively coupled plasma optical emission spectroscopy (ICP-OES; Avio 200) was used to analyze the ratio of Co and Ce atom.

Electron paramagnetic resonance (EPR) measurements were performed at 77 K on a Bruker A300 spectrometer, employing a modulation frequency of 100 kHz and a modulation amplitude of 1.0 G.

X-ray photoelectron spectroscopy (XPS) measurements were carried out on an AXIS Ultra DLD spectrometer (Kratos, UK) using Al Kα radiation.

H_2-TPR was performed on a TP-5076 dynamic sorption analyser. Each sample (100 mg) was pre-treated in He at 450 °C for 1 h, reduced in 5 vol % H_2/N_2 for 1h/3h, cooled to 30 °C in He, and

exposed to O_2 for 40 min. After switching back to 5 vol % H_2/N_2, the temperature was raised from 30 to 900 °C at 10 °C min^{-1} and the consumption profile was recorded. The H_2 consumption corresponding to surface oxygen (30-200 °C) and lattice oxygen (200-900 °C) was determined from the TPR profiles. The migration rate of surface oxygen for the treated sample was calculated as[1]:

$$Surface\ oxygen\ migration = \frac{H_2^a - H_2^b}{2}$$

H_2^a and H_2^b denote the H_2 consumption of surface oxygen in the untreated and treated samples, respectively.

Similarly, the migration rate of lattice oxygen for the treated sample was calculated as:

$$Lattice\ oxygen\ migration = \frac{H_2^c - H_2^d}{2}$$

H_2^c and H_2^d denote the H_2 consumption of lattice oxygen in the untreated and treated samples, respectively.

The O_2 temperature-programmed desorption (O_2-TPD) experiment was carried out in the same device as H_2-TPR and the test procedure was similar. 100mg sample was pretreated in He at 450 °C for 1 h, then cooled to 80 °C. The atmosphere was switched to 5 % O_2/N_2 for adsorption for 40 min, followed by switching back to He. Temperature-programmed desorption (TPD) was then performed by heating to 900 °C, and the desorption profile was recorded. **The $^{18}O_2$-TPD** was as same as O_2-TPD experiment, except the 5 % O_2/He was replaced with 1 % $^{18}O_2$/He. The adsorption temperature of $^{18}O_2$ was 120 °C. The signals at *m/z* = 32, 34 and 36 corresponding to $^{16}O_2$, $^{16}O^{18}O$ and $^{18}O_2$, respectively, were recorded by a MS detector (Hiden EXQ, UK) during the heating ramp. **The NO + $^{18}O_2$-TPD** measurements were conducted using a similar procedure, except that the adsorption step was performed at 120 °C with NO + $^{18}O_2$ for 40min. The signals corresponding to $^{16}O_2$, $^{16}O^{18}O$ and $^{18}O_2$ (m/z = 32, 34, and 36), as well as NO^{16} and $NO^{16}O^{16}$ (m/z = 30 and 46), were monitored using the mass spectrometer.

For **the He temperature-programmed desorption (He-TPD)** experiment, 100mg sample was pretreated in the flow of He at 200°C for 1 h to remove the impurity and then programmed to be heated to 900 °C with 10 °C/min under He flow. The signal of oxygen (m/z = 32) was detected using the mass spectrometer.

For the **NO temperature-programmed desorption (NO-TPD)** experiment, 100mg sample was pretreated in the flow of He at 200°C or 500°C for 1 h to remove the impurity and then

programmed to be heated to 900 °C with 10 °C/min under He flow. The signal of NO (m/z = 32) was detected using the mass spectrometer.

Thermogravimetric analysis (TG) was conducted on a TGA/DSC 3 + 1 LF (METTLER TOLEDO, Switzerland) thermogravimeter. 10mg sample was heated in N_2 (50 mL/min) to 600 °C before switching to 21% O_2/N_2 (50 mL/min) and maintained for 30 min, then switched to 5% H_2/N_2 (50 mL/min) and maintained for 40 min, and then switched again to 21% O_2/N_2 for 20 min, and the cyclic process was repeated twice.

The oxygen storage capacity (OSC) of the samples was measured via the O_2 pulse injection method. Samples were first reduced at 500 °C under 5 vol.% H_2/N_2 (30 mL min^{-1}) for 1 h, then cooled to 120 °C under He (40 mL/min). Successive pulses of pure O_2 were introduced at 2 min intervals until no additional oxygen uptake was observed. OSC values were calculated using the following equation:

$$OSC\ (\mu mol/g) = \frac{H \times P \times V}{R \times T \times M}$$

H — Accumulated signal peak.

P(kPa) — Atmospheric pressure.

R(J/mol·K) — Ideal Gas Constant.

T(K) — Temperature.

M(g) — Sample mass.

V(μL) — pulse volume.

NO/O_2 pulse experiments were performed using a cyclic multi-pulse (NO/O_2) method. A 0.1 g sample was activated in He at 450 °C for 1 h and then cooled to 300 °C. Alternating pulses of 4% NO and 2% O_2 were introduced, with each cycle consisting of 30s NO followed by 30s O_2, at a total flow rate of 200 mL/min. The concentrations of NO, O_2, and NO_2 were continuously monitored using an online mass spectrometer (Hiden EXQ, UK). **The NO pulse** experiment was conducted in a similar manner to the NO/ O_2 pulse procedure, except that only NO pulses were introduced without alternating with O_2.

In situ DRIFTS spectroscopy was performed on an INVENIO-S spectrometer (Bruker, USA) equipped with an MCT detector. Powder samples were loaded into a reaction cell with KBr

windows, and the total gas flow was maintained at 100 mL/min. For the NO + O_2 adsorption–storage, samples were activated in He at 450 °C for 1 h with a heating rate of 10 °C/min. Background spectra were collected over 120-400 °C. The samples were then exposed to a NO + O_2 atmosphere for 20 min, during which adsorption spectra were recorded at intervals. After adsorption, the flow was switched to He for 20 min purging, followed by heating to 400 °C at 10 °C/min to record desorption spectra. For O_2 adsorption experiments, the same procedure was employed, except that the NO + O_2 mixture was replaced with O_2.

Section S3: Supplementary table data

Table S1. The high-activity temperature window (T_{90}) of NH_3-SCR catalysts

Catalyst	T_{90} (℃)	Ref
$MnCeO_x$	100-300	2
$WO_3/CeZrO_2$	222-454	3
WO_3/ $CeZrO_x$ (κ-$Ce_2Zr_2O_8$)	250-475	4
$CeZrO_x$-Cu/SSZ-13	175-550	5
Cu/SSZ-13	200-550	6
$MoWO_x/CeO_2$	200-375	7
$Ce1Sn_aNb_1O_x$	225-500	8
Cu/SSZ-13	200-500	9
CeO_2/Cu-SSZ-13	200-550	10

Table S2. NO_x adsorption-storage performance of different types of PNA materials

PNA Materials	Adsorption Temperature (℃)	Adsorption time (min)	NO_x Adsorption (μmol/g)	Desorption temperature (℃)	Ref
Co/CZ-0.01M	120	10	172.5	250-400	This work
Ce/BEA	120	30	130.0	200-400	11
$Mn/CeZrO_x$	120	10	65.0	130-250、250-400	12
$Cu/Ba/Al_2O_3$	150	180	78.0	200-400、400-700	13
BaMn/SSZ-13	100	15	255	100-250	14

Pt-Pd/CZ	120	15	37.0	300-500	15
$CoMgAlO_x$	100	180	250.0	150-350、350-600	16
$Mn/CeZrO_x$	120	10	68.4	180.335	17
$CoAlO_x$	120	60	150.0	100-400	18
Co_3O_4	100	20	49.3	200-450	19
Pd/SSZ-13@Al_2O_3	100	20	80.0	200-400	20
Pd/SSZ-13	120	10	57.3	150-450	21
Pd/SSZ-13	100	20	110.0	100-200	22

Table S3. Texture properties of the samples

Sample	$S_{BET}(m^2/g)$	Total Pore volume(mL/g)	Average pore radius(nm)
Co/CZ	65	0.35	10.0
Co/CZ-0.005M	64	0.33	10.1
Co/CZ-0.01M	69	0.32	9.2
Co/CZ-0.05M	68	0.33	9.7
Co/CZ-0.1M	67	0.27	8.0

Table S4. Elemental composition obtained by the ICP

Sample	Co (wt%)	Ce (wt%)
Co/CZ	3.88	56.1
Co/CZ-0.01M	3.46	57.0

Table S5. Oxygen vacancy concentration of samples

Sample	Oxygen vacancy concentration (10^{13}spins/g)
Co/CZ-0.01M	2.661
Co/CZ	1.733

Semi-quantification requires calibration using a standard sample with a known spin concentration. Under identical measurement conditions, the EPR spectrum of the standard is recorded, and the double-integrated area is correlated with the number of spins to establish a calibration curve. The double-integrated area of the sample is then applied to this curve to calculate the absolute number of spins, which is divided by the sample mass to obtain the oxygen vacancy concentration in units of spins per gram (spins/g). Here, the spin concentration refers to the number of paramagnetic centers per unit mass of sample. Specifically, the absolute spin concentration N_s is determined using the following equation.

$$Ns = \frac{DI\,V}{P_{1/2}\,B_m\,Q\,c\,S(S+1)\,n_B f(B_1,B_m)}$$

DI = Double Integral c = Resonator Calibration Factor

V = Sample Volume S = Electron Spin

P = Microwave Power n_B = Boltzmann Factor

B_m= Modulation Amplitude $f(B_1,B_m)$ = Resonator Field Profile

Q = Resonator Q-factor

The calculation involves acquisition parameters, the physical dimensions of the sample, and the characteristic properties of the resonator. The acquisition parameters are stored together with the experimental spectrum along with the resonator properties, which are set by a factory calibration of the resonator with a standard of known concentration. Using the above semi-quantification method, the oxygen vacancy concentrations of the samples were accurately determined (Table S5). Co/CZ-0.01M exhibits a significantly higher oxygen vacancy concentration than Co/CZ.

Section S4: Supplementary Figures

Fig S1: Reproducibility tests

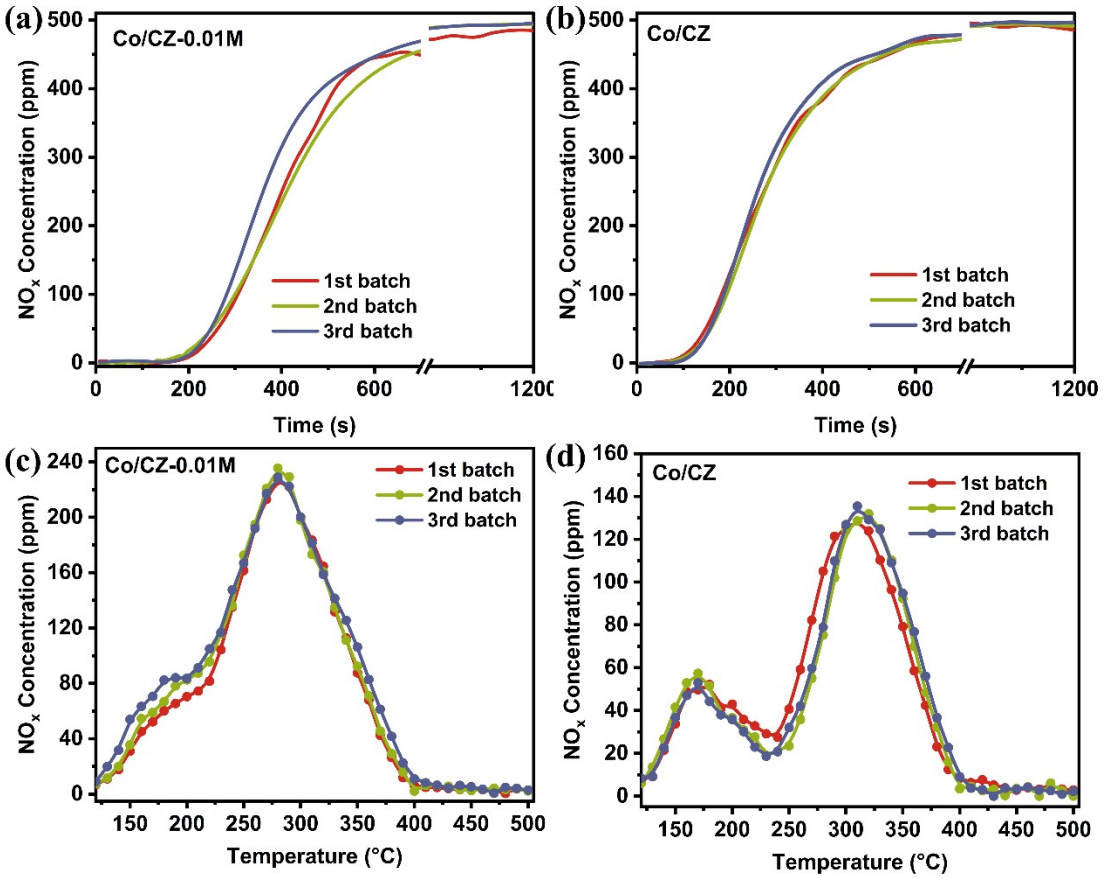

Fig. 1. NO_x adsorption curves of (a) Co/CZ-0.01M and (b) CoCZ; NO_x-TPD of (c) Co/CZ-0.01M, and (d) CoCZ. The data presented were based on three separate material syntheses. Catalytic activity was then evaluated using the same testing protocol for each batch.

Fig S2: NO_x-TPD curves

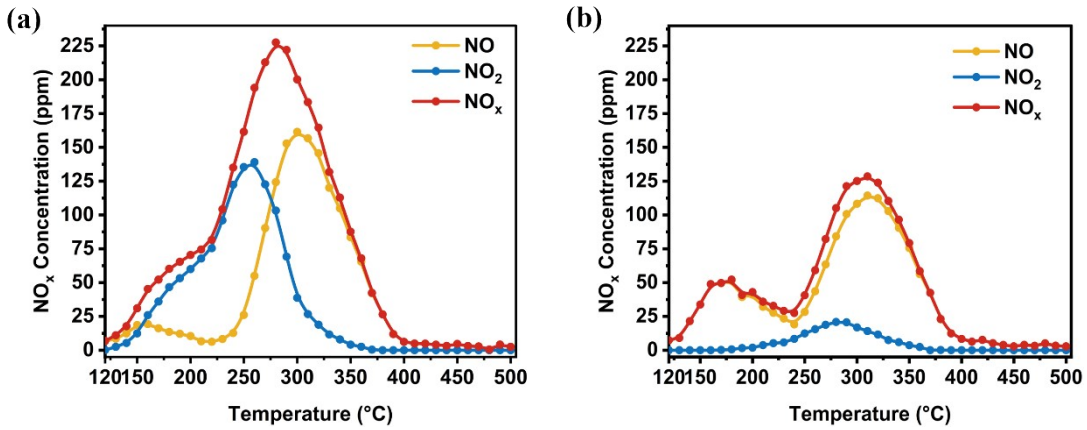

Fig. S2. Variations in NO/NO_2 concentration during NO_x desorption for (a) Co/CZ-0.01M, (b) Co/CZ

Fig S3: NO_x adsorption-storage performance under different NO/O_2 introduction sequences

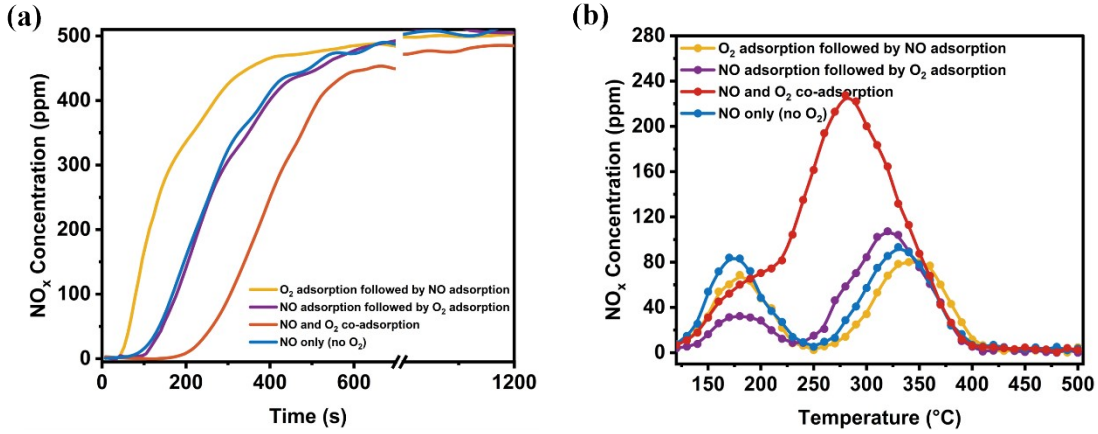

Fig. S3. (a) NO_x adsorption curves of Co/CZ-0.01M; (b) NO_x-TPD of Co/CZ-0.01M.

Fig S4: NO_x adsorption-storage performance under wet conditions

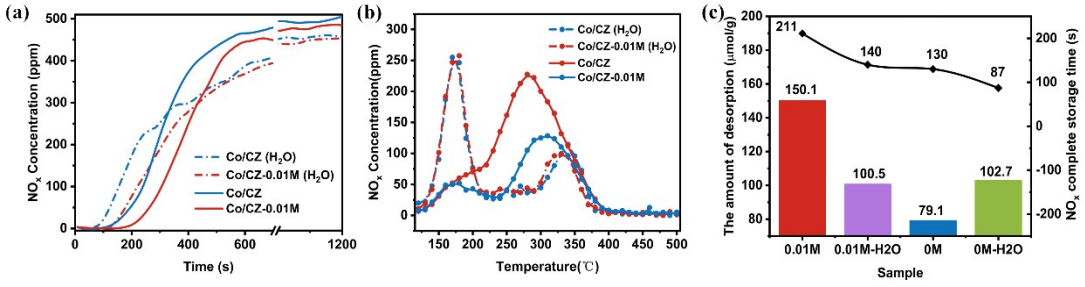

Fig. S4. (a) NO_x adsorption curves of Co/CZ-0.01M; (b) NO_x-TPD of Co/CZ-0.01M. (c) NO_x

desorption capacity. Adsorption conditions: 500 ppm of NO, 10 vol %O_2, 5%H_2O, N_2 as balance, total flow rate of 420 mL/min.

Fig S5: Multiple storage-desorption cycles of Co/CZ-0.01M

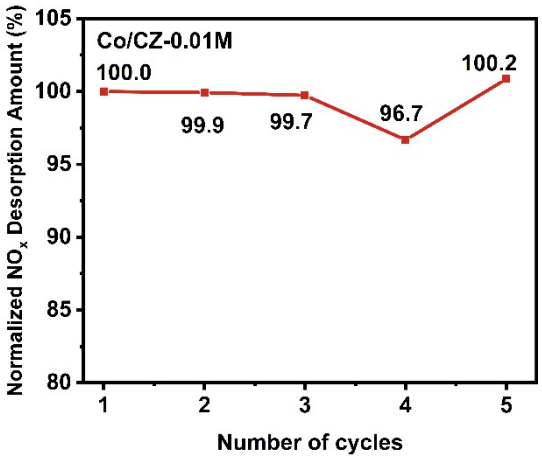

Fig. S5. Multiple storage-desorption cycles of Co/CZ-0.01M

Fig S6: XPS spectra

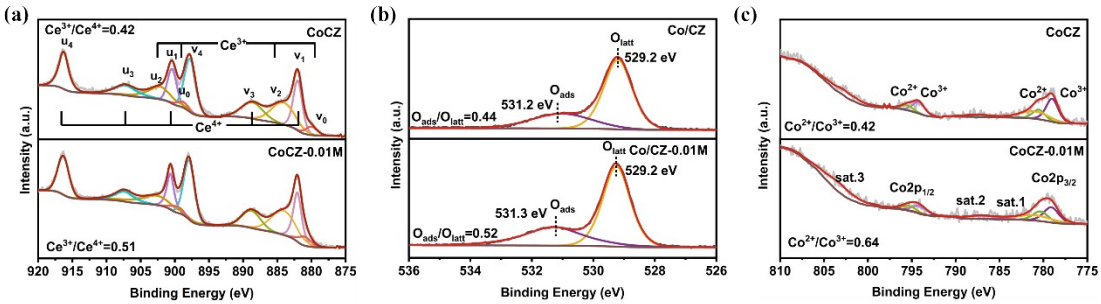

Fig. S6. XPS spectra of (a) Ce 3d, (b) O 1s and (c) Co 2p for samples.

Fig S7: Peak area of integral O_2-TPD

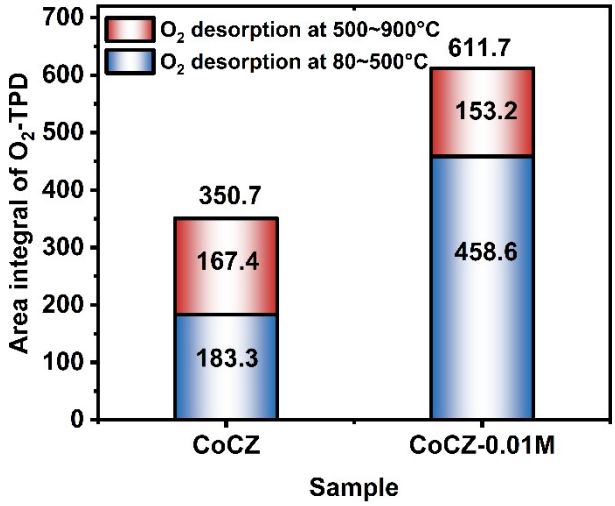

Fig. S7. Peak area of integral O_2-TPD.

Fig S8: Designed H_2-TPR profiles

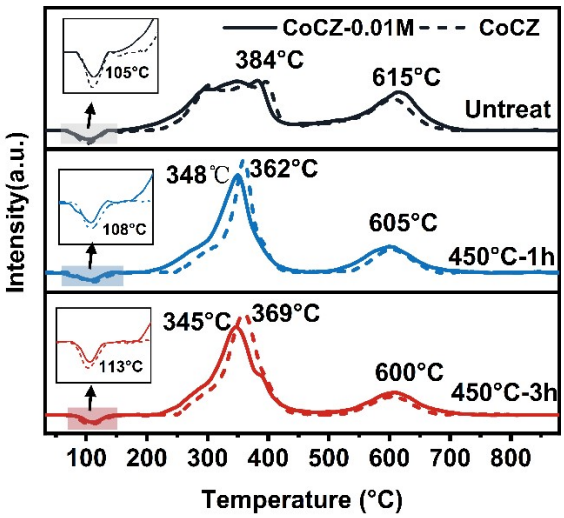

Fig. S8. Designed H_2-TPR profiles.

Fig S9: H_2-TPR profiles of samples.

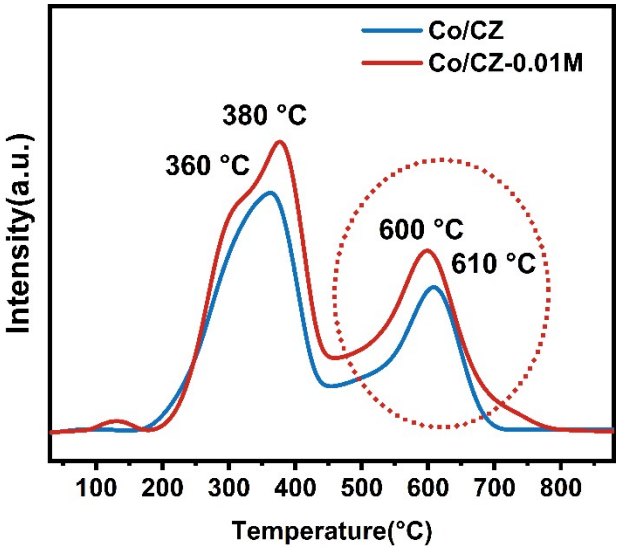

Fig. S9 H_2-TPR profiles of samples.

Both Co/CZ and Co/CZ-0.01M exhibit two distinct reduction peaks: the low-temperature peak at ca.380 °C, attributed to the consumption of surface-labile oxygen species and the transformation of Co_3O_4 to CoO. The high-temperature peak occurs at ca. 600 °C and corresponds to the deep reduction of bulk lattice oxygen [23, 24]. The TG test aims to assess the impact of acid-etching modification on lattice oxygen mobility. Therefore, a temperature that effectively activates and probes bulk lattice oxygen is required. The selected 600 °C corresponds to the onset of significant lattice oxygen

activation and migration. H_2–O_2 alternating experiments conducted at this temperature provide a direct evaluation of the catalyst's bulk oxygen reservoir and its replenishment kinetics during redox cycles.

Fig S10: NO_x adsorption-storage performance after pretreatment at 600 °C for 3 h

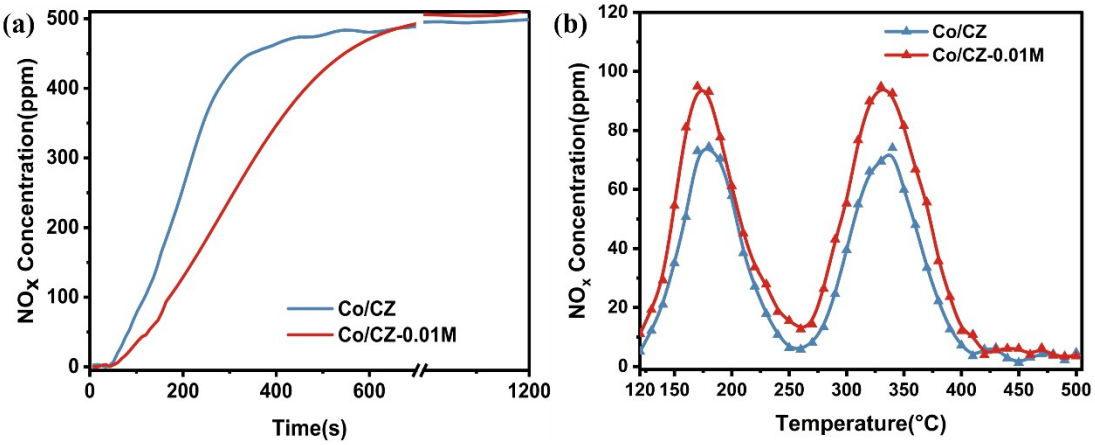

Fig. S10. (a) NO_x adsorption curves; (b) NO_x-TPD.

Fig S11: Isotope $^{18}O_2$-TPD curves after amplification

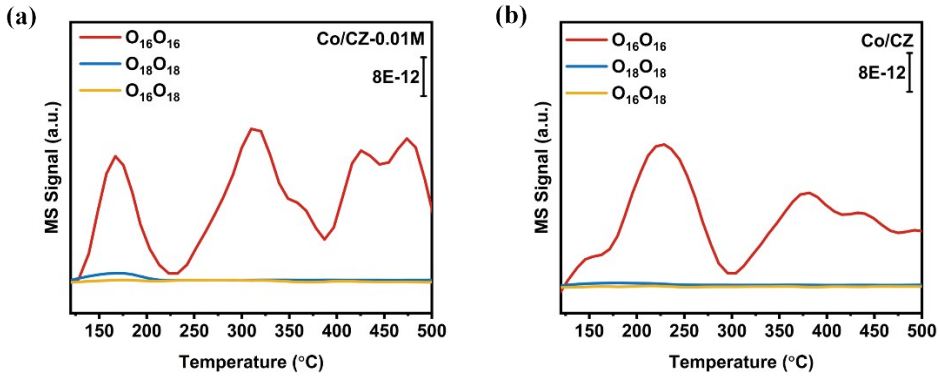

Fig. S11. Isotope $^{18}O_2$-TPD curve of (a) Co/CZ-0.01M, (b) Co/CZ after amplification.

Fig S12: NO pulse curves

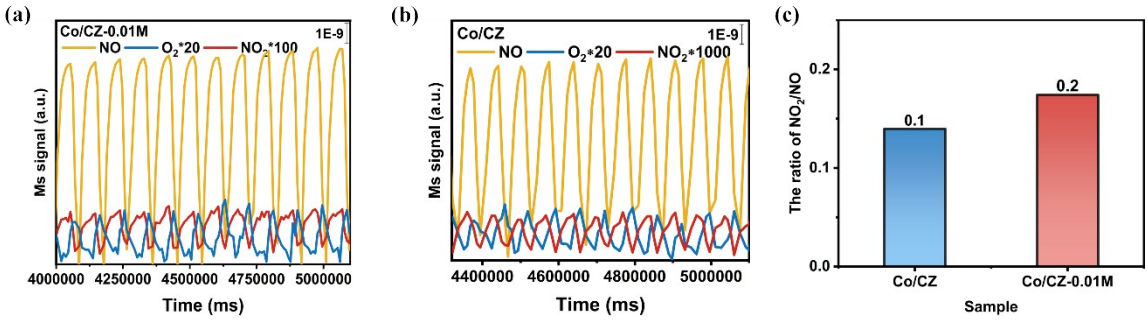

Fig. S12. NO pulse curves of (a) Co/CZ-0.01M and (b) Co/CZ; (c) The ratio of NO_2 to NO generated in NO pulses.

Fig S13: The ratio of NO_2 to NO generated in NO/O_2 pulses

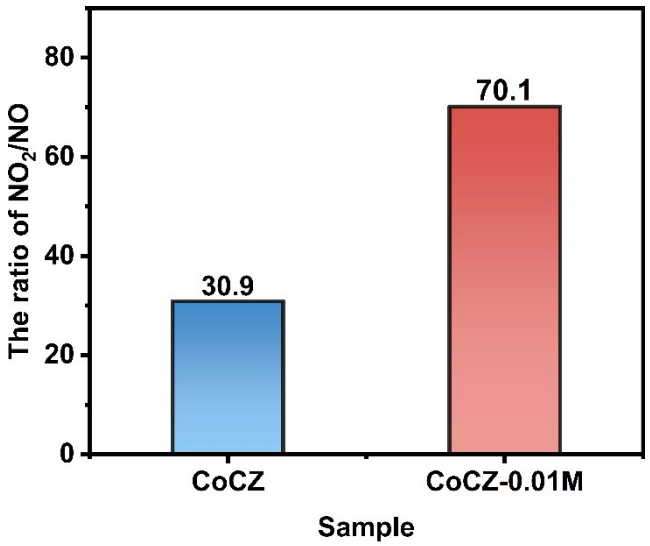

Fig. S13. The ratio of NO_2 to NO generated in NO/O_2 pulses.

Fig S14: In situ DRIFTS spectra of $NO+O_2$ adsorption

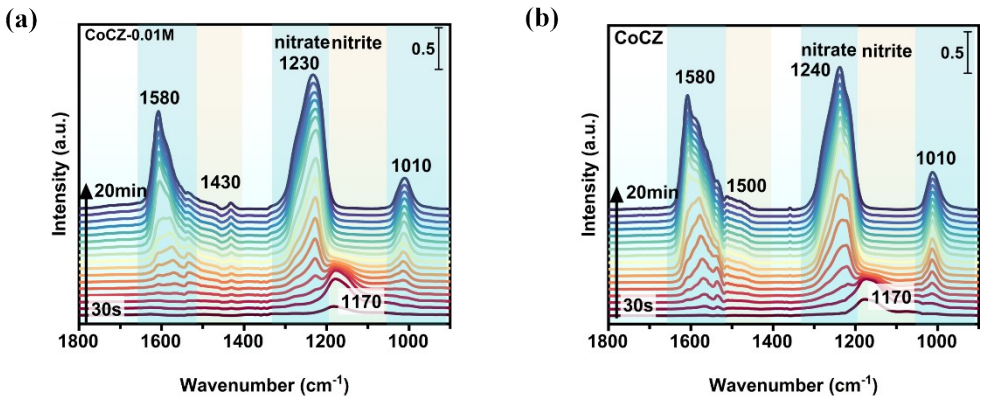

Fig. S14. In situ DRIFTS spectra of $NO+O_2$ adsorption collected at 120℃ on (a) Co/CZ-0.01M and (b) Co/CZ.

Reference

1. D. Chen, D. He, J. Lu, L. Zhong, F. Liu, J. Liu, J. Yu, G. Wan, S. He and Y. Luo, Appl. Catal. B Environ, 2017, **218**, 249-259.
2. L. Wang, X. Li, S. Ren, M. Liu, X. Wang, W. Wang, C. He, S. Chai, C. Zheng, X. Li and Y. Chai, Sep. Purif. Technol., 2025, **379**, 135179.
3. S. Liu, P. Yao, Q. Lin, S. Xu, M. Pei, J. Wang, H. Xu and Y. Chen, Catal. Today, 2021, **382**, 34-41.
4. S. Liu, Y. Huang, S. Li, Q. Lin, J. Wang, S. Xie, F. Liu, H. Xu and Y. Chen, Environ. Sci. Technol., 2023, **57**, 16685-16694.
5. S. Xu, J. Li, Q. Lin, H. Xu, J. Wang and Y. Chen, Chem. Eng. J., 2023, **476**, 146767.
6. X. Hu, J. Lin, X. Tan, C. Lin, Y. Zhang and W. Shan, Chem. Eng. J., 2025, **520**, 165978.
7. X. Han, L. Jiang, Z. Zhang, K. Liu, M. Bian, Z. Yuan, Y. Li, C. Rao, X. Yang and Y. Zhang, Environ. Sci. Technol., 2025, **59**, 12364-12377.
8. Y. Zhu, J. Liu, G. He, S. Xie, W. Shan, Z. Lian, F. Liu and H. He, Engineering, 2025, **48**, 141-150.
9. W. Lv, F. Sun, W. Jiao, H. Zhao, X. Li, R. Zhang, Y. Guo, J. Jia and B. Lv, Catal. Sci. Technol., 2025, **15**, 3762-3772.
10. Z. Liu, M. Shen, S. Wang, C. Zhang, J. Wang, W. Li and F. Gao, ACS Catal., 2025, **15**, 12927-12943.
11. X. Li, M. Shen, C. Zhang, Y. Wang, X. Li, L. Jia, F. Gao, W. Li, L. Yang and G. Shen, J. Hazard. Mater., 2026, **503**, 140983.
12. L. Yang, M. Shen, F. Gao, W. Li, G. Shen and X. Li, Sep. Purif. Technol., 2025, **361**, 131483.
13. H. Kim, H. Jung, J. W. Han and K. B. Lee, Chem. Eng. J., 2022, **429**, 132112.
14. Z. Chen, M. Qin, Y. Xie, Y. Guo, C. Dong, C. Wang and Y.-H. Qin, J. Hazard. Mater., 2025, **488**, 137327.
15. Y. Ji, D. Xu, S. Bai, U. Graham, M. Crocker, B. Chen, C. Shi, D. Harris, D. Scapens and J. Darab, Ind. Eng. Chem. Res., 2016, **56**, 111-125.
16. Y. Choi, K. T. Lee and K. B. Lee, Sep. Purif. Technol., 2023, **324**, 124391.
17. L. Yang, M. Shen, X. Li, L. Jia, F. Gao, W. Li, X. Li and G. Shen, Sep. Purif. Technol., 2026, **382**, 135923.
18. R. Yang, Y. Cui, Q. Yan, C. Zhang, L. Qiu, D. O'Hare and Q. Wang, Chem. Eng. J, 2017, **326**, 656-666.
19. J. Cai, S. Hao, Y. Zhang, X. Wu, Z. Li and H. Zhao, Chin. J. Chem. Eng., 2024, **66**, 1-7.
20. X. Chen, M. Nan, J. Huang, L. Li, Z. Zhang and G. Yang, Environ. Sci. Technol., 2025, **59**, 20546-20556.
21. Y. Wang, X. Shi, Z. Liu, Y. Shan, W. Shi, Y. Yu and H. He, Appl. Catal. B Environ, 2023, **324**, 122254.
22. Y. Wang, X. Zhao, T. Chen, Z. Zheng, R. Zhan and H. Lin, Fuel, 2024, **358**.
23. J. Xu, G. Lu, Y. Guo, Y. Guo and X.-Q. Gong, Appl. Catal. A-Gen., 2017, **535**, 1-8.
24. J. Liu, H. Wang, W. Zhang, J. Gao, Q. Yu, J. Ke and L. Wang, Fuel, 2023, **349**, 128657.